

Intra-pulse H₂O Absorption Diagnostic for Temperature Sensing in a Rapid Compression Machine

Ehson F. Nasir, Aamir Farooq*

King Abdullah University of Science and Technology, Clean Combustion Research Center (CCRC), Physical Science and Engineering Division (PSE), Thuwal 23955-6900, Saudi Arabia

*Corresponding Author: aamir.farooq@kaust.edu.sa

Abstract

An *in-situ* temperature diagnostic based on intra-pulse absorption spectroscopy has been developed using two pulsed quantum cascade lasers (QCLs) centered at 5.46 and 5.60 μm for rapid compression machine (RCM) experiments. Pulsed mode operation of the QCLs yielded a broad spectral tuning range (1.8 – 2.3 cm^{-1}), through which spectral line-shapes of two H₂O ro-vibrational transitions were resolved at high pressure conditions in the RCM (15 – 20 bar). Based on the resolved line-shapes, a calibration-free two-line thermometry method was used to determine the gas temperature. A high temporal resolution of 10 μs was achieved through a pulse repetition frequency of 100 kHz. The diagnostic was validated through measurements of temperature rise during the first-stage ignition of n-pentane/air mixtures. Thereafter, temperature rise during the first-stage ignition of iso-octane/air mixtures was quantified for the first time and compared with the calculated temperature rise using a chemical kinetic model.

Keywords: Rapid compression machine; Quantum cascade laser; Absorption spectroscopy.

1. Introduction

Rapid compression machines (RCMs) are used to investigate the chemistry of fuel auto-ignition at low temperatures (< 1000 K) and at pressures relevant to practical internal combustion engines (10 – 40 bar) [1,2]. Under these conditions, many hydrocarbon fuels exhibit two-stage ignition wherein a small heat release event precedes the main ignition event [3–7]. Due to the need for measurements to solely be sensitive to chemical effects, RCMs are designed to provide a near homogeneous, adiabatic gas-phase environment. This allows for the measurements to be compared directly with kinetic models without the additional complexity of considering transport effects. In cases of two-stage ignition, however, the first-stage heat release has been shown to affect predictions of temperature rise as well as timing of the second-stage ignition [8]. It is, therefore, important to quantify the temperature rise during first-stage ignition through a sensitive *in-situ* temperature diagnostic.

The development of semiconductor laser technology has enabled access to the near- and mid-infrared wavelength region for spectroscopic applications. Through the absorption spectroscopy technique, the mid-infrared region can be leveraged to obtain highly sensitive measurements of molecular concentration and temperature. The high temporal resolution afforded by laser absorption diagnostic is ideally suited to transient reactors such as shock tube and the RCM where the experimental timescale is generally of the order of milliseconds. The absorption technique has been successfully applied previously to high-temperature kinetics experiments in shock tubes for determining temperature rise during the oxidation of hydrocarbon fuels [9].

In recent years, temperature measurements in the RCM with the use of semiconductor laser sources have been demonstrated. Sung and co-workers applied an external cavity quantum cascade laser (QCL) to measure temperature using two ro-vibrational transitions of water vapor in the mid-

infrared near $7.6 \mu\text{m}$ [10,11] with a temporal resolution of 5 ms and a spectral tuning range of 1.4 cm^{-1} . Higher tuning ranges are achievable in the near infrared through either supercontinuum sources [12], or through a recent application of dual-frequency comb spectrometers [13], although near-infrared spectroscopic lines provide much smaller detection sensitivity than those in the mid-infrared. Moreover, while near-infrared diode lasers have been shown to provide high temporal resolution measurements up to 1 MHz through wavelength scanning [14–16], the spectral tuning range available at such high scan frequencies is usually very small [9], which may not be sufficient to resolve line-shapes at high pressure conditions.

Recently in our group, temperature diagnostics based on pulsed mid-infrared QCLs were demonstrated with a high temporal resolution in both shock tube [17,18] and RCM experiments [19]. For the shock tube application, Chrystie et al. developed a temperature diagnostic by accessing multiple H_2O lines with a single QCL [17]. Though the lines were closely spaced, the diagnostic was used for low pressures ($\sim 1 - 2 \text{ bar}$) at which the lines remained distinguishable. The H_2O lines also had lower-state energies (E'') up to 3654 cm^{-1} for-high temperature conditions (1000 – 2000 K) in the shock tube. Moreover, the relatively large line-width associated with pulsed mode operation affected the overall broadening of the H_2O lines. These characteristics of the diagnostic developed by Chrystie et al. had to be adjusted for temperature sensing in the RCM. Since RCMs are typically operated at much higher pressures (10 – 20 bar), the pulsed laser line-width is relatively negligible to the pressure broadening. However, due to the high pressure, the lines used for temperature sensing must be sufficiently spaced, ideally in separate wavelength regions. The lines must also have low E'' for higher detection sensitivity at the lower temperature conditions typical of RCM experiments (700 – 950 K). The previous work on temperature sensing in the RCM [19] relied on seeding carbon monoxide, the target molecule, to monitor temperature

rise during first-stage ignition. Since CO is a reactive molecule in the context of gas-phase combustion, a temperature diagnostic based on an inert molecule is preferable to prevent chemical effects of the seeded gas.

A temperature diagnostic using water vapor transitions is demonstrated in this work, for application to rapid compression machines, based on the methodology of pulsed QCL absorption [19]. The diagnostic improves upon the previous H₂O diagnostic by Chrystie et al. [17] by utilizing two separate QCLs accessing two widely separated lines with relatively low E'' . The sensor is applied here to two-stage ignition of iso-octane in the RCM.

2. Experimental Method

2.1. Rapid Compression Machine

The RCM used in this work is a twin-opposed piston facility and can provide end-of-compression pressures between 10 – 40 bar. The combustion chamber of the RCM has a bore of 50.8 mm and contains two ports for optical access, a third port for pressure transducer (Kistler 6045A) and a fourth one for gas exchange to the mixing vessels and manifold. Heating jackets are used to vary the initial temperature of the combustion chamber. The piston heads of the RCM are creviced to create a homogeneous adiabatic core gas within the combustion chamber. Based on the adiabatic core assumption, end-of-compression (EOC) temperature can be inferred from the pressure trace using the following isentropic relation:

$$\int_{T_0}^T \frac{\gamma}{\gamma-1} \frac{dT}{T} = \ln\left(\frac{P}{P_0}\right) \quad (1)$$

The RCM can provide EOC temperatures over 550 – 950 K by varying the initial temperature and through the use of different diluent gases. For a more detailed description of the RCM facility, the reader is encouraged to refer to reference [20].

2.2. Absorption Spectroscopy

The methodology for the laser diagnostic developed in this work is similar to the previously published work on temperature sensing using carbon monoxide [19]. Here, we discuss it very briefly. The diagnostic is based on the principles of absorption spectroscopy, as governed by the Beer-Lambert relation:

$$\frac{I_0}{I_t} = \exp(PXLS\phi) = \exp(\alpha) \quad (2)$$

In Eq. 2, S and ϕ refer to the spectroscopic parameters, line-strength and line-shape function, of the molecular transition of interest while L is the path-length of laser propagation through the test gas. P refers to the total pressure of the gas while X refers to the mole fraction of the target species of interest. Together, the product of these quantities is the absorbance (α) and is determined by measuring the ratio of incident and transmitted laser intensities (I_0 and I_t).

The dependence of absorbance on the line-shape function (ϕ) in Eq. 2 may be removed by measuring the integrated area of the absorption line, yielding simply:

$$A = PXLS \quad (3)$$

The line-strength is only a function of temperature and thus by measuring the integrated areas of two separate absorption lines, the dependence on other parameters can be dropped by taking the ratio R :

$$R = \frac{A_1}{A_2} = \frac{S_1(T)}{S_2(T)} \quad (4)$$

The temperature can then be determined from the following expression where E'' is the lower state energy of the absorption transition:

$$T = \frac{\frac{hc}{k}(E_2'' - E_1'')}{\ln R + \ln \frac{S_2(T_0)}{S_1(T_0)} + \frac{hc}{k} \left(\frac{E_2'' - E_1''}{T_0} \right)} \quad (5)$$

In Eq. 5, non-linear terms arising from stimulated emission have been dropped for simplicity [21]. The effect on temperature determination from the omission of those terms is between 0.2 – 0.5% over the temperature range of interest (700 – 950 K) and much smaller than the other uncertainties associated with the diagnostic (see section 3). From Eq. 5, it can be discerned that the measured temperature is only dependent on the measured area ratio and spectroscopic parameters (S, E'') which can be determined from databases such as HITRAN. Therefore, the temperature measurement is completely calibration-free, unaffected by other gas properties.

2.3. Temperature Diagnostic

In this work, molecular transitions of water vapor near 5.46 μm (1785 cm^{-1}) and 5.60 μm (1833 cm^{-1}) were to measure gas temperature in the RCM. The spectroscopic parameters of these lines were taken from the HITRAN database [22] and are provided in Table 1. The lines were selected based on the criteria set out in [23] to avoid interference from other transitions as well as providing high signal-to-noise ratio. Although two closely-spaced absorption lines are present near both 1785 and 1833 cm^{-1} , the two lines at each wavelength can be treated as effectively one line, for the purpose of the area ratio in Eq. 5, due to the very small differences in their lower-state energies and the large overlap resulting from collisional broadening at high pressures.

Table 1. Spectroscopic parameters of the selected H₂O absorption lines.

Line-center (cm^{-1})	Line Strength (HITRAN units)	Lower State Energy (cm^{-1})
1784.887	7.874×10^{-21}	920.2098

1784.971	2.363×10^{-20}	920.1680
1833.278	1.462×10^{-21}	1557.8470
1833.286	4.872×10^{-22}	1557.8436

For a temperature diagnostic based on two-line thermometry, the sensitivity of the measured area ratio to changes in temperature should be maximized. This sensitivity can be determined by differentiating Eq. 5 with respect to temperature to yield the following expression:

$$\text{Sensitivity} = \frac{dR/R}{dT/T} = \frac{\frac{hc}{k}(E_2^* - E_1^*)}{T} \quad (6)$$

The sensitivity of the area ratio should ideally be larger than one over the temperature range of interest. Figure 1 shows that the calculated sensitivity is > 1 for temperatures lower than 900 K which are of interest in this work for first-stage ignition of iso-octane.

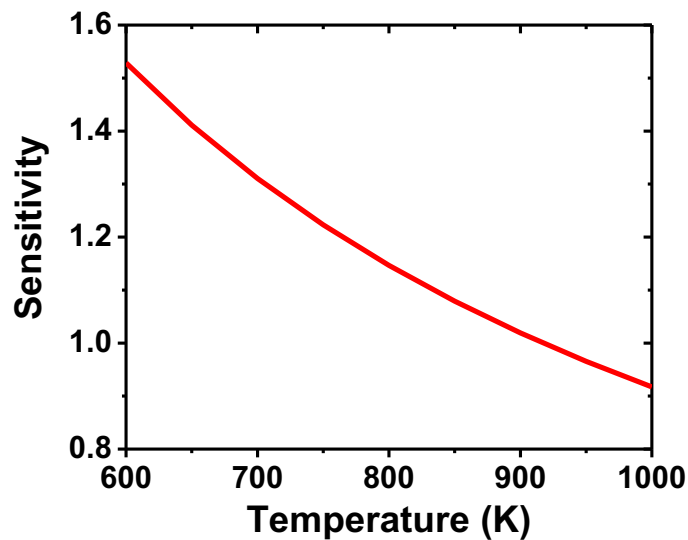


Figure 1. Sensitivity of the area ratio as a function of temperature for the line pair used in this work.

Two distributed feedback pulsed QCLs from Alpes Lasers, centered near 5.46 μm and 5.60 μm , were used to access the targeted H_2O transitions in this work. The lasers were aligned on a collinear path through the RCM, as shown in Fig. 2. At room temperature, the H_2O lines exhibit very strong absorption from ambient water vapor. Therefore, to avoid the laser signal being completely lost to the water vapor in ambient air, the laser beam path was purged with nitrogen gas.

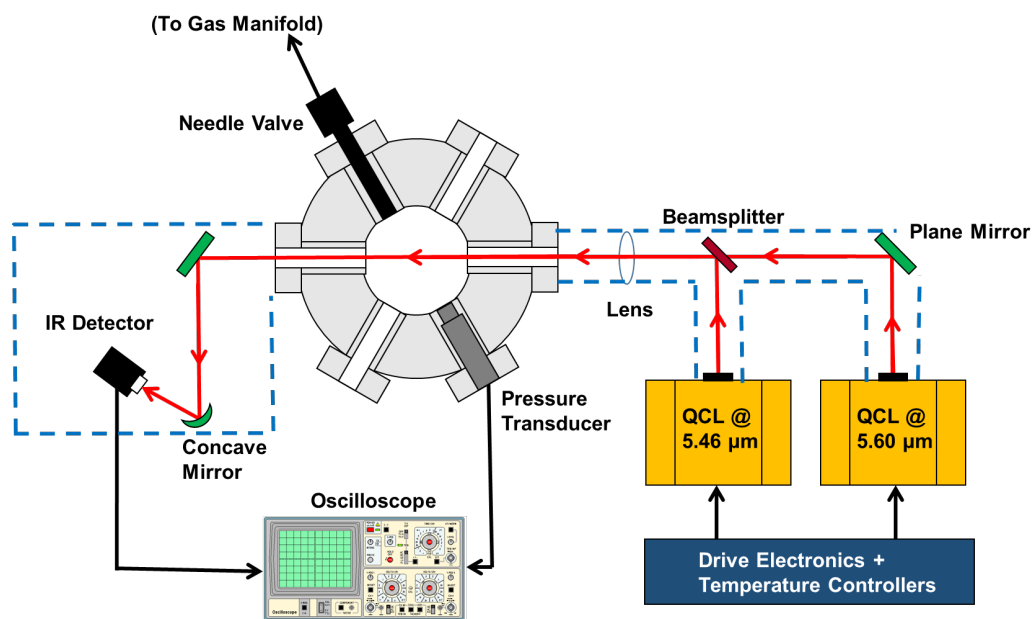


Figure 2. Schematic of the laser alignment through the cross-section of the RCM combustion chamber. The dashed blue lines show the N_2 -purged area to minimize ambient absorption.

The laser signals were captured on a high bandwidth (500 MHz) MCT mid-infrared detector by Vigo Systems and sampled at 250 MHz with a Tektronix oscilloscope. The QCLs were operated in pulsed mode at 100 kHz repetition frequency, resulting in an effective temporal resolution of 10 μs . Due to the differences in operating characteristics of the two QCLs, different pulse durations were used to maximize the tuning range resulting from the intra-pulse down-chirp. Figure 3 provides a representative intensity trace for the two lasers and their respective tuning ranges (1.75 and 2.30 cm^{-1}). The tuning ranges of both QCLs were sufficient to resolve the line-shapes of the

targeted H₂O lines. The two laser pulses were separated in time by approximately 5 μ s, so their signals can be distinguished using a single detector. The detector signal between laser pulses was used to determine any background thermal emission, which was subtracted from the main signal prior to processing. The incident laser signal was measured prior to each experiment in vacuum and was used as the I_0 in Eq. 2. To reduce beam steering noise from mechanical vibrations, the laser beams were focused into the center of the RCM through a plano-convex lens and tests with non-absorbing nitrogen gas were performed in the RCM to verify the laser signal quality.

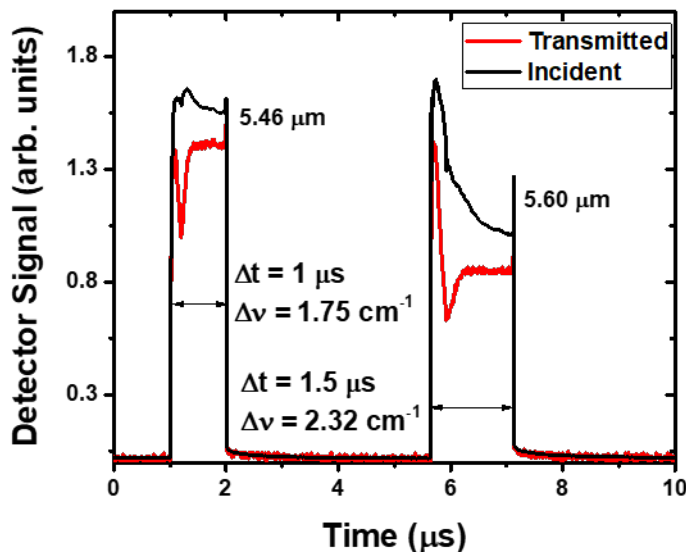


Figure 3. Representative incident and transmitted laser intensity traces measured at EOC. The transmitted signal exhibits absorption due to water vapor. EOC Conditions: $T = 676$ K, $P = 14.8$ bar; iso-octane/air, $\phi = 1$ with 1.5% H₂O seeded.

The average chirp rate used in this work is lower than that used in the previous intra-pulse temperature diagnostic [19] due to the pulse durations being larger and the overall tuning range being lower than that in the previous work. From the previous work, the upper limit of laser line-

width in pulsed mode operation was found to be 0.016 cm^{-1} . Compared to the minimum collisional width of H_2O lines in this work at 10 bar ($\sim 0.25 \text{ cm}^{-1}$), the laser line-width is significantly smaller and will not affect the application of the Beer-Lambert law.

3. Results and Discussion

In this work, molecular transitions of water vapor near $5.46 \mu\text{m}$ (1785 cm^{-1}) and $5.60 \mu\text{m}$ (1833 cm^{-1}) were selected to measure gas temperature in the RCM. Two sets of experiments were performed in the RCM, one using n-pentane/air mixtures and the other using iso-octane/air mixtures. In both sets of experiments, a stoichiometric equivalence ratio was used ($\phi = 1$) and water vapor was seeded into the mixture up to a mole fraction of 1.5%. The gas mixtures were prepared manometrically in a mixing vessel wherein pure water vapor was injected prior to other mixture components. Since water is essentially inert at the temperatures of this work, seeding of water vapor should not affect the chemistry. Such small amounts of water vapor will also not alter the overall 3rd-body collision efficiency parameters.

A representative H_2O absorption spectra is shown in Fig. 4 where the measured profile is fit with a Voigt function to determine the integrated area. The relatively small residuals between the measured and fitted profiles indicate that Voigt fitting is suitable for these conditions. The uncertainty in temperature measurements from the Voigt fit is $< 5\%$.

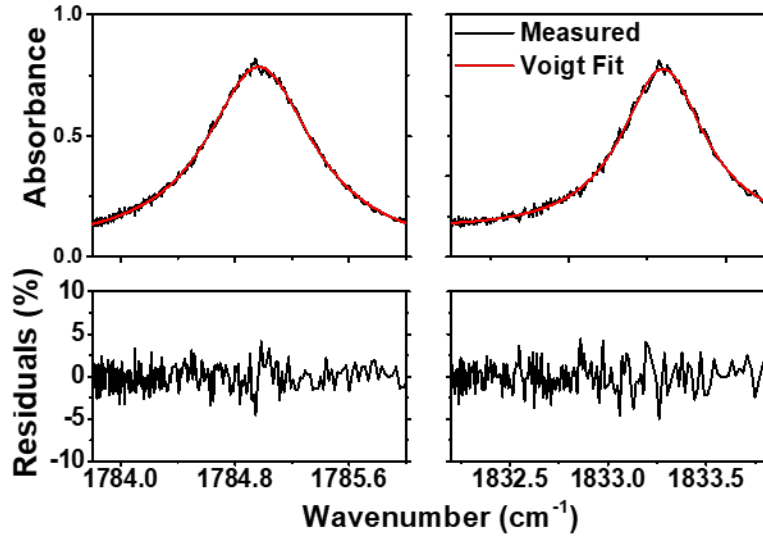


Figure 4. Representative measured H₂O spectra at EOC along with Voigt fits. EOC Conditions: $T = 676$ K, $P = 14.8$ bar; iso-octane/air, $\phi = 1$ with 1.5% H₂O seeded.

The line-strengths in Eq. 5 were obtained from the HITRAN database with a stated uncertainty of 10%. The uncertainty in line-strength propagates to approximately 10.1% uncertainty in measured temperature at 800 K. The uncertainty contribution from thermal boundary layer within the combustion chamber is 2% of the measured temperature, as discussed in [19]. The overall uncertainty in temperature measurement is estimated, via root-sum-square, to be about 11.4%. It should be noted the major component in this overall uncertainty is the contribution from the tabulated line-strength. Given that the EOC temperatures determined through the laser diagnostic were within 5% of the temperatures determined using the isentropic relation, we believe that our measurement uncertainty is reasonably small.

Figure 5 shows two measured temperature traces, labelled as ‘laser’, from experiments in n-pentane/air mixtures. The measured temperature trace is overlaid with simulated temperature using the chemical kinetic model by Bugler et al. [24]. The temperature traces are filtered with a

low-pass filter at 1 kHz to remove the high-frequency noise associated with pulse-to-pulse variation and Voigt fit errors. Zero on the time axis represents EOC and the first sharp temperature rise after EOC represents first-stage ignition while the second sharp temperature rise corresponds to the second-stage ignition. The measured temperature rise during first-stage ignition is lower than the simulated temperature rise and concurs with the results from the previous temperature diagnostic based on carbon monoxide [19]. At the onset of second-stage ignition, the temperature measurement is unreliable due to signal saturation.

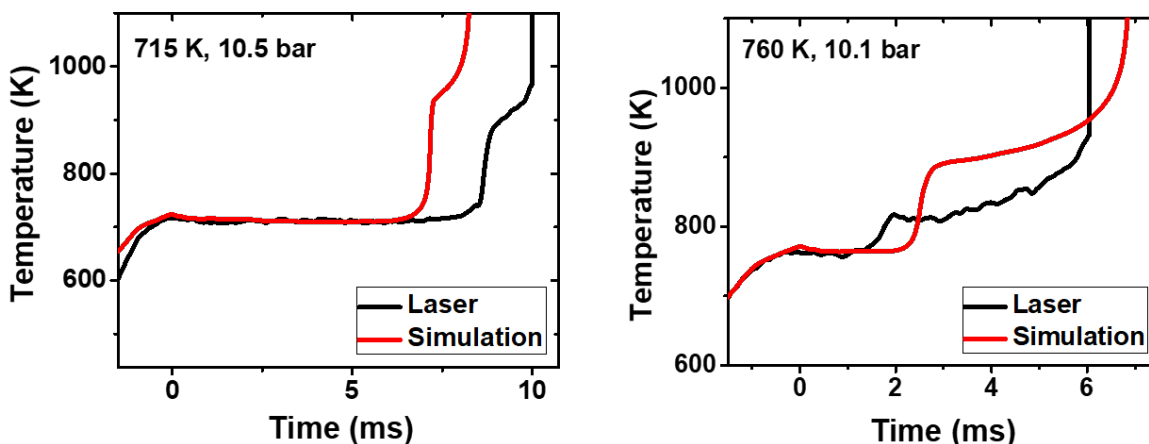


Figure 5. Measured temperature traces overlaid with simulated temperature from Bugler et al. [24] model. Conditions used: n-pentane/air, $\phi = 1$ with 1.5% H₂O seeded.

Having confirmed previously obtained results, the temperature diagnostic was then applied to iso-octane oxidation experiments in a similar manner to the n-pentane experiments. Experiments were performed at nominal pressures of 15 and 20 bar and in the temperature range corresponding to two-stage ignition of iso-octane (670 – 735 K). Figure 6 shows measured temperature traces from four separate experiments. The measured temperature traces are compared with simulated temperature traces using the chemical kinetic models for iso-octane combustion by LLNL [25] and by Atef et al. [26]. For all of the cases shown in Fig. 6, the measured temperature rise during first-

stage ignition is greater than that predicted by either the LLNL or Atef models. The LLNL model generally predicts a higher temperature rise than the Atef model.

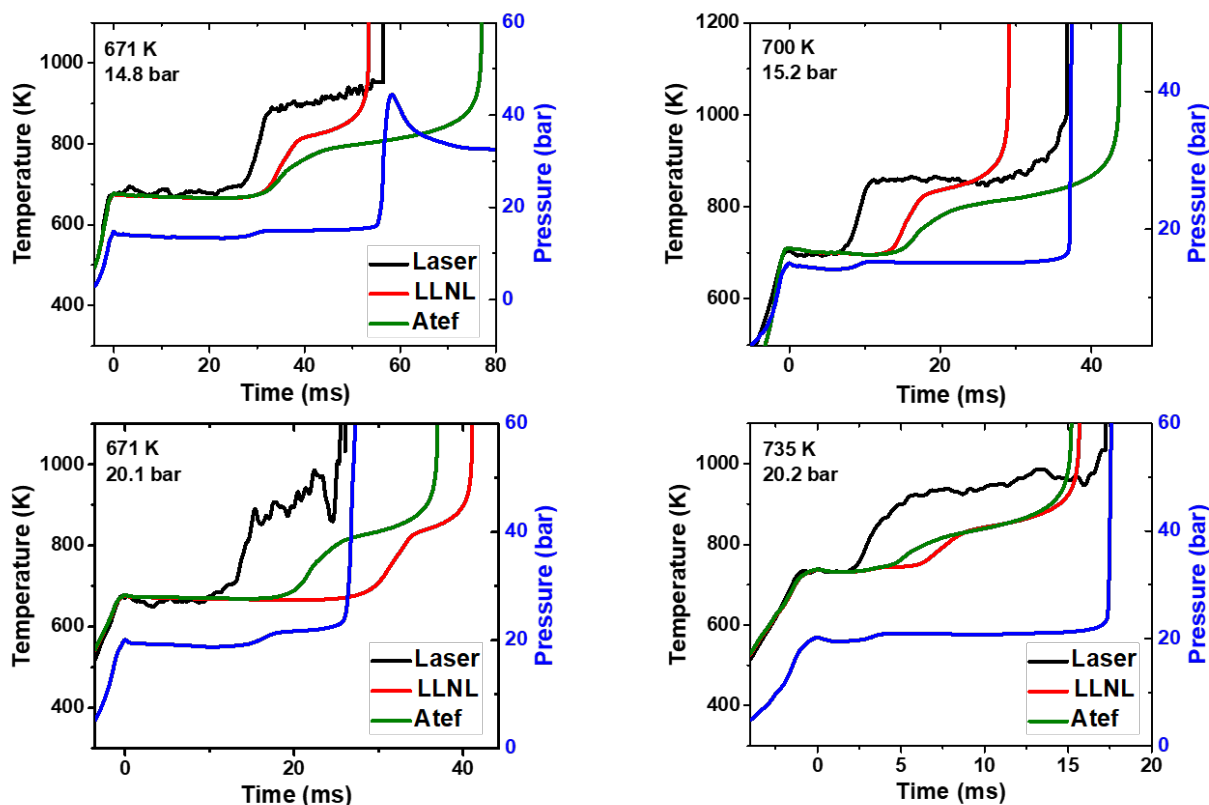


Figure 6. Measured temperature traces overlaid with simulated temperature from LLNL [25] and Atef et al. [26]. Conditions used: iso-octane/air, $\phi = 1$ with 1.5% H_2O seeded. EOC temperature and pressure are annotated within each plot. Pressure traces shown in blue.

It may be noted that while the onset of first-stage ignition measured experimentally is consistently faster than model predictions, the onset of second-stage ignition does not follow a clear trend and may be earlier or later than model predictions. The results from the iso-octane experiments are contrary to the trends seen in the n-pentane experiments. Based on the previous work on temperature sensing in the RCM [19], it was expected that the zero-dimensional kinetic models will overpredict temperature rise during first-stage ignition due to the presence of boundary layer

and other transport effects in the actual experiments. Since the current diagnostic confirms this for n-pentane but not for iso-octane, it may suggest that kinetic models for iso-octane underestimate the heat release during first-stage ignition. A further investigation of kinetic models may be needed to pin down the source of this discrepancy.

4. Conclusion

A high temporal resolution, calibration-free temperature diagnostic was developed based on water vapor transitions in the mid-infrared. Pulsed mode operation of QCLs enabled high temporal resolution at 100 kHz as well as large intra-pulse spectral tuning ($1.8 \text{ cm}^{-1} - 2.3 \text{ cm}^{-1}$). The latter allowed for the application of the calibration-free two-line thermometry technique by measuring integrated areas of the absorption lines. Water vapor was seeded to the initial fuel/air mixture to measure temperature during first-stage ignition. The diagnostic was first applied to cases of stoichiometric n-pentane oxidation in the rapid compression machine at a nominal pressure of 10 bar to validate against previous work [19] and then applied to cases of iso-octane oxidation at nominal pressures of 15 and 20 bar. For both fuels, the temperature rise during first-stage ignition was quantified and compared against the latest chemical kinetic models. The iso-octane results showed that the measured first-stage temperature rise was consistently higher than that predicted by models. A more detailed analysis of the uncertainties in heat release prediction by kinetic models may be needed to address this discrepancy.

Acknowledgement: The research reported in this work was funded by the Office of Sponsored Research (OSR) at King Abdullah University of Science and Technology (KAUST).

References

1. C. J. Sung and H. J. Curran, *Prog. Energy Combust. Sci.* **44**, 1 (2014).
2. S. S. Goldsborough, S. Hochgreb, G. Vanhove, M. S. Wooldridge, H. J. Curran, and C.-J. Sung, *Prog. Energy Combust. Sci.* **63**, 1 (2017).
3. R. Minetti, M. Carlier, M. Ribaucour, E. Therssen, and L. R. Sochet, *Combust. Flame* **102**, 298 (1995).
4. K. Fieweger, R. Blumenthal, and G. Adomeit, *Combust. Flame* **109**, 599 (1997).
5. J. Herzler, L. Jerig, and P. Roth, *Proc. Combust. Inst.* **30**, 1147 (2005).
6. G. Vanhove, G. Petit, and R. Minetti, *Combust. Flame* **145**, 521 (2006).
7. P. Zhang, W. Ji, T. He, X. He, Z. Wang, B. Yang, and C. K. Law, *Combust. Flame* **167**, 14 (2016).
8. S. S. Goldsborough, G. Mittal, and C. Banyon, *Proc. Combust. Inst.* **34**, 685 (2013).
9. C. S. Goldenstein, R. M. Spearrin, J. B. Jeffries, and R. K. Hanson, *Prog. Energy Combust. Sci.* **60**, 132 (2017).
10. M. Uddi, A. K. Das, and C.-J. Sung, *Appl. Opt.* **51**, 5464 (2012).
11. A. K. Das, M. Uddi, and C.-J. Sung, *Combust. Flame* **159**, 3493 (2012).
12. T. Werblinski, F. Mittmann, M. Altenhoff, T. Seeger, L. Zigan, and S. Will, *Appl. Phys. B* **118**, 153 (2015).
13. A. D. Draper, R. K. Cole, A. S. Makowiecki, J. Mohr, A. Zdanowicz, A. Marchese, N. Hoghooghi, and G. B. Rieker, *Opt. Express* **27**, 10814 (2019).

14. C. S. Goldenstein, C. L. Strand, I. A. Schultz, K. Sun, J. B. Jeffries, and R. K. Hanson, *Appl. Opt.* **53**, 356 (2014).
15. C. S. Goldenstein, C. A. Almodóvar, J. B. Jeffries, R. K. Hanson, and C. M. Brophy, *Meas. Sci. Technol.* **25**, 105104 (2014).
16. G. C. Mathews and C. S. Goldenstein, in *AIAA Scitech 2019 Forum* (American Institute of Aeronautics and Astronautics, 2019).
17. R. S. M. Chrystie, E. F. Nasir, and A. Farooq, *Proc. Combust. Inst.* **35**, 3757 (2015).
18. R. S. M. Chrystie, E. F. Nasir, and A. Farooq, *Opt. Lett.* **39**, 6620 (2014).
19. E. F. Nasir and A. Farooq, *Proc. Combust. Inst.* **36**, 4453 (2017).
20. E. F. Nasir, *Mid-IR Laser Absorption Diagnostics for Shock Tube and Rapid Compression Machine Experiments*, King Abdullah University of Science and Technology, 2018.
21. R. K. Hanson, R. M. Spearrin, and C. S. Goldenstein, in *Spectrosc. Opt. Diagnostics Gases* (Springer, 2016), pp. 107–129.
22. I. E. Gordon, L. S. Rothman, C. Hill, R. V Kochanov, Y. Tan, P. F. Bernath, M. Birk, V. Boudon, A. Campargue, K. V Chance, B. J. Drouin, J. M. Flaud, R. R. Gamache, J. T. Hodges, D. Jacquemart, V. I. Perevalov, A. Perrin, K. P. Shine, M. A. H. Smith, J. Tennyson, G. C. Toon, H. Tran, V. G. Tyuterev, A. Barbe, A. G. Császár, V. M. Devi, T. Furtenbacher, J. J. Harrison, J. M. Hartmann, A. Jolly, T. J. Johnson, T. Karman, I. Kleiner, A. A. Kyuberis, J. Loos, O. M. Lyulin, S. T. Massie, S. N. Mikhailenko, N. Moazzen-Ahmadi, H. S. P. Müller, O. V Naumenko, A. V Nikitin, O. L. Polyansky, M. Rey, M. Rotger, S. W. Sharpe, K. Sung, E. Starikova, S. A. Tashkun, J. Vander Auwera, G. Wagner, J. Wilzewski, P. Wcisło, S. Yu, and E. J. Zak, *J. Quant.*

Spectrosc. Radiat. Transf. **203**, 3 (2017).

23. A. Farooq, J. B. Jeffries, and R. K. Hanson, Meas. Sci. Technol. **19**, 75604 (2008).

24. J. Bugler, A. Rodriguez, O. Herbinet, F. Battin-Leclerc, C. Togbé, G. Dayma, P. Dagaut, and H. J. Curran, Proc. Combust. Inst. **36**, 441 (2017).

25. H. J. Curran, P. Gaffuri, W. J. Pitz, and C. K. Westbrook, Combust. Flame **129**, 253 (2002).

26. N. Atef, G. Kukkadapu, S. Y. Mohamed, M. Al Rashidi, C. Banyon, M. Mehl, K. A. Heufer, E. F. Nasir, A. Alfazazi, A. K. Das, C. K. Westbrook, W. J. Pitz, T. Lu, A. Farooq, C.-J. Sung, H. J. Curran, and S. M. Sarathy, Combust. Flame **178**, 111 (2017).